Conditioning of Cardiovascular Tissue Using a Noncontact Magnetic Stretch Bioreactor with Embedded Magnetic Nanoparticles

Matthew Hogan,[†] Yi-Ting Chen,[‡] Arati G. Kolhatkar,[‡] Christopher J. Candelari,[†] Sridhar Madala,[§] T. Randall Lee,[‡] and Ravi Birla*,[†]

[†]Department of Biomedical Engineering, Science and Engineering Research Center (SERC-Building 545), University of Houston, 3605 Cullen Boulevard, Room 2027, Houston, Texas 77204-5060, United States

[‡]Department of Chemistry, Science and Engineering Research Center (SERC-Building 545), University of Houston, 3605 Cullen Boulevard, Room 5004, Houston, Texas 77204-5060, United States

[§]Indus Instruments, 721 Tristar Drive, Webster, Texas 77598, United States

Ⓢ Supporting Information

ABSTRACT: Bioreactor systems, an integral component of tissue engineering, are designed to simulate complex in vivo conditions to impart functionality to artificial tissue. All standard forms of stretch bioreactors require physical contact with artificial heart muscle (AHM). However, we believe that noncontact stretch bioreactors have the potential to lead to higher functional benefit of AHM. Our work is focused on the fabrication of a noncontact magnetic stretch bioreactor (MSB) that uses magnetic nanoparticles to simulate stretch conditions to impart functionality. During our development of this system, we applied magnetically induced stretch conditioning through application of an oscillating magnetic field to a ferromagnetic heart muscle model. Fibrin scaffolds were loaded with magnetic nanoparticles prior to tissue model formation. Oscillating magnetic fields were applied by a novel bioreactor system through displacement of a neodymium magnet. The addition of commercially obtained iron(III) oxide (Fe_2O_3) in sufficient quantities to allow for physiologically relevant stretches (15% axial displacement) caused toxic effects after 4 days of culture. In contrast, loading scaffolds with monodispersed, high-saturation-magnetization magnetite (Fe_3O_4) nanoparticles specifically prepared for these experiments increased the field strength of the magnetized fibrin 10-fold over polydispersed, low-saturation magnetization, Fe_2O_3. Additionally, loading with Fe_3O_4 enabled magnetically actuated stretching with markedly reduced toxicity over 8 days of culture. Using a 20% stretch 0.5 Hz protocol, we observed a significant increase in twitch force over controls at days 4 and 6. This work provides a technology for controlled noncontact mechanical stretch to condition AHM.

KEYWORDS: bioreactors, cardiovascular, tissue engineering, stretch conditioning, magnetic nanoparticles
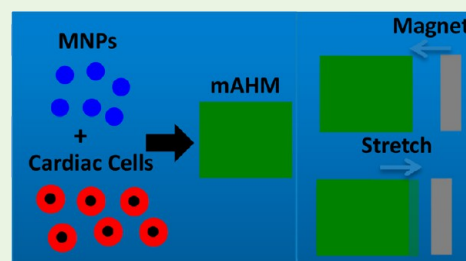
1. INTRODUCTION

Heart failure is a leading cause of death worldwide, and there remains an unprecedented need to develop innovative treatment strategies.[1] More than 3 million people live with heart disease in the United States alone, and managing these patients accrues annual costs of nearly $320 billion.[2] Given that cardiac muscle tissue exhibits limited regenerative capability, a viable tissue-engineered muscle replacement/supplement to augment contractile function might serve as a bridge, or even alternative treatment, to heart transplant. There have been several seminal studies in the field that have successfully generated cardiac patches. The first model of 3D heart muscle was published in 1997 and based on the culture of chick cardiac myocytes in a 3D collagen matrix.[3] Another seminal publication in the field, also in 1997, demonstrated the fabrication of 3D heart muscle tissue on a synthetic polymer scaffold, nonwoven polyglycolic acid (PGA).[4] Furthermore, successful generation of a physiologically relevant tissue-engineered heart muscle will be an important first step in the creation of a true tissue-engineered whole heart. To this end, researchers in the field of tissue engineering have focused on the development and maintenance of in vitro 3D heart muscle tissue that replicates the functional performance of mammalian heart muscle.[5]

There have been several studies describing the fabrication of artificial heart muscle.[6−13] One of the models developed by our group, three-dimensional artificial heart muscle (3D-AHM), is based on spontaneous delamination of a monolayer of primary neonatal cardiac cells that are distributed within a fibrin gel network.[14] In this approach, cardiac cells are plated on a tissue culture surface that is coated with a layer of fibrin gel. Spontaneous contractions of the cell monolayer leads to compaction of the fibrin gel and the formation of functional 3D artificial heart muscle. AHM can be electrically stimulated to generate twitch forces of over 4 mN and can also be electrically paced at frequencies of 1−7 Hz without fatigue.[14]

Several studies have found a positive correlation between stretch and heart muscle function.[15−18] Under normal physiological conditions, the heart responds to changes in hemodynamic loads by increasing the extracellular matrix components in addition to hypertrophic and hyperplasic growth of the cardiac cells.[19] Fink et al. utilized a mechanical stretch regime to study changes in 3D cardiac muscle that was engineered by culturing neonatal cardiac cells within a collagen gel; this was the first time that stretch was used to condition 3D heart muscle.[15] The constructs were subjected to a 20% stretch protocol at a frequency of 1.5 Hz for a period of 6 days, which led to a doubling of the twitch force. In addition, mechanical stretch led to an increase in calcium sensitivity and β-adrenergic response.[20] The Akyhari group utilized a model of 3D heart muscle by culturing cells, obtained from human hearts, in a gelatin sponge. Subjecting these constructs to 20% stretch at 1.33 Hz frequency for 14 days led to an increase in cell proliferation;[16] contractile properties were not evaluated in this study. A seminal publication in the field described the noncontact stretch of 3D heart muscle tissue.[18] In this study, 3D heart muscle was fabricated by culturing primary cardiac myocytes in 3D scaffolds that were fabricated using knitted fabric. A novel noncontact bioreactor, fabricated using electromagnets, was described in this study. Noncontact stretch of 3D heart muscle tissue resulted in an increase in collagen synthesis, along many other metrics that were measured. This study was seminal in the field, as it was the first description of noncontact stretch of 3D heart muscle tissue. In vitro tissue-engineered cardiac muscle models generally exhibit lower morphological and functional cellular maturity compared to native cardiac muscle. Increases in collagen deposition as well as hyperplastic and hypertrophic growth can be achieved via controlled stretch regimens.[16,21]

The strategy of magnetic force-based tissue engineering (Mag-TE) has demonstrated the applicability of magnetic nanoparticles (MNPs) in various aspects of tissue engineering, such as magnetofection, magnetic cell patterning, and the fabrication of tissue-like constructs.[22,23] Magnetic fields have been used to support the formation of cell sheets, to regulate 3D spatial distribution of cells within scaffolds, to support 3D levitation of isolated cells, and to form 3D tissue.[24−27] The successful formation of functional tissue remains challenging, but the incorporation of MNPs in cells/tissues/scaffolds allows for magnetic force-based manipulation of these components to build more complex systems.[28] Another approach to the use of MNPs is mechanotransduction -- a pathway by which physical stimulus is converted into biochemical activity or function; for example, the production of a functional tissue matrix from mechanical stimuli to the cells.[28] Incorporation of MNPs in scaffolds followed by the application of tensile or compressive forces using a magnetic field has been shown to induce functionality in certain cells (e.g., the differentiation of stem cells or proliferation of mucosa cells).[29] This approach has also been pursued by the stimulation of magnetically responsive scaffolds with an alternating magnetic field to develop mature myocardial tissue from neonatal rat cardiac cells.[30] Further, the concept of maturation of tissue engineered concepts has been explored with magnetic bioreactor compression of bone tissue analogs.[31] Our application built upon this prior research by developing a bioreactor for the calibrated use of magnetic fields for the controlled stretch of 3D heart muscle. Although magnetic fields have been used in various aspects of tissue

engineering, our novel application has led to the development of a noncontact magnetically guided stretch bioreactor.

Stretch is a known modulator of heart muscle function, and work by our group, and others, have demonstrated a positive correlation between stretch and heart muscle function.[15,16,32] Work using bioengineered heart muscle has demonstrated a positive correlation between uniaxial stretch and connexxin43 expression, electrical conduction velocity, intracellular calcium transients, contractile properties, expression of contractile and junction proteins and cellular alignment. Stretch protocols for bioengineered heart muscle have varied: 7−14 days, 5−20% stretch and 1−5 Hz stretch frequency. This body of work has clearly demonstrated a positive correlation between uniaxial stretch and 3D heart muscle function. Building upon this work, our objective was to develop a noncontact magnetic stretch bioreactor to condition 3D heart muscle tissue.

The objectives of this study were:[1] to develop the methodology for fabrication of magnetic AHM (mAHM),[2] to fabricate a noncontact magnetic stretch bioreactor (MSB), and[3] to condition mAHM in our MSB using noncontact stretch protocols. To the best of our knowledge, this work is the first demonstration of neodymium magnet-based fields to be used for noncontact stretch of magnetic AHM. In this paper, we report optimized culture conditions to support the fabrication of mAHM and the development of enhanced functionality in the AHM using MNPs embedded in the fibrin gel component of the noncontact MSBs. This unique noncontact-based technology can also be extended to other tissue systems and is a significant advance compared to the current state of the art in the field.

2. MATERIALS AND METHODS

All animal protocols were approved by the Institutional Animal Care and Use Committee (IACUC) at the University of Houston, in accordance with the *Guide for the Care and Use of Laboratory Animals* (NIH Publication No. 86−23, 1996). All chemicals, reagents, and solvents were purchased from Sigma-Aldrich (St. Louis, MO, USA) unless otherwise specified. The chemicals used in the syntheses and characterization studies were of analytical grade and were used as received from the supplier without further purification. Millipore water (resistivity of >18 MΩ cm) obtained from a Milli-Q water system and filtered through a 0.22 μm filter membrane was used during the synthesis and washing steps in the preparation of the MNPs. All glassware and equipment used in the synthesis of the MNPs were cleaned in an aqua regia solution and rinsed with Milli-Q water prior to use.

2.1. Isolation of Primary Cardiac Cells. Primary cardiac cells were extracted from the hearts of 2−3 day old neonatal Sprague−Dawley rats using an established method.[7] Hearts were minced and placed in a 60 mm Petri dish filled with ice cold PBS. Tissue was then washed to remove blood and minced to a final size of approximately 1 mm³, then transferred to a dissociation solution (DS) and incubated for 30 min with gentle shaking. Supernatant was then collected and added to 3 mL of horse serum and then spun at 1000 rpm. The cell pellets were then resuspended in 5 mL of horse serum. Bulk tissue was resuspended in DS and the process was repeated for a total of 3−4 digestions. Collected cells were combined, centrifuged, and resuspended in culture media (CM).[14]

2.2. Fabrication of Artificial Heart Muscle. We fabricated AHM using a previously published protocol.[14] Briefly, 35 mm culture dishes were coated with 2 mL of SYLGARD (PDMS, type 184 silicone elastomer; Dow Chemical, Midland, MI, USA) and allowed to air-dry. Four minutien pins were inserted into the PDMS layer to form a 2 cm x 2 cm square. A fibrin scaffold was formed by mixing 1 mL of 10 U/mL thrombin in CM with 500 μL of 20 mg/mL fibrinogen in saline together in a prepared 35 mm Petri dish. Cell laden CM was then
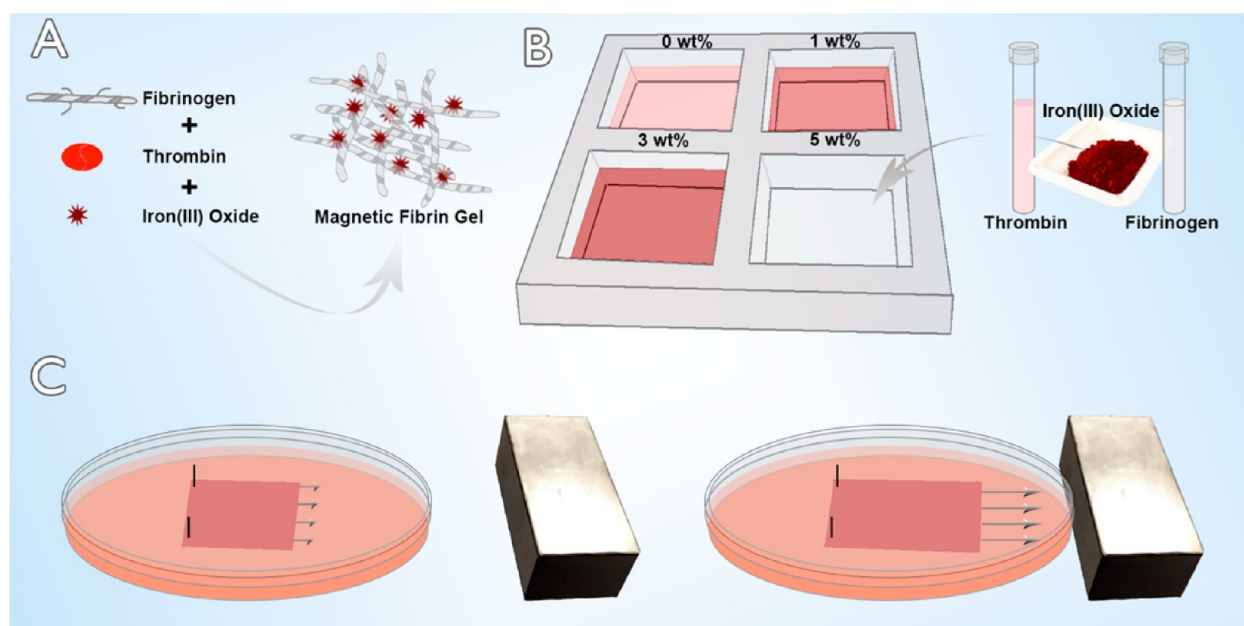
Figure 1. Schematic illustration of the stretch bioreactor concept: (A) iron(III) oxide becomes trapped in fibrin gel, (B) the scaffold is loaded with different amounts of iron, and (C) the magnetic force effects are tested with a fixed strength neodymium magnet.

added to the Petri dish with PDMS, pins and fibrin and incubated at 37 °C.

2.3. Synthesis of Fe_3O_4 Magnetic Nanoparticles (MNPs). The Fe_3O_4 MNPs were synthesized by a modification of a procedure reported by Deng et al.[33] in which a 150 mL round-bottomed pressure vessel was charged with $FeCl_3 \cdot 6H_2O$ (4.2 g) in 30 mL of ethylene glycol, followed by the addition of sodium acetate (3.08 g); with the latter addition leading to a rapid change in the color of the solution from orange to brown. The solution was then stirred for 30 min, followed by the addition of polyethylene glycol (0.50 g) in 20 mL of ethylene glycol. The flask was sealed by a Teflon cap and heated at 188 °C for 21 h. The black precipitate obtained was separated using a strong bar magnet, washed with three cycles each of ethanol and water, and then redispersed in ethanol. The synthesized particles formed a powder upon drying at 40 °C and were set aside for future use. To obtain MNPs of varying size, we adjusted the concentrations of the starting materials and diethylene glycol.[33]

2.4. Characterization of MNPs. The MNPs were characterized by scanning electron microscopy (SEM; LEO-1525 operating at 15 kV) and vibrating sample magnetometry (VSM; LakeShore VSM 7300 Series with LakeShore 735 Controller and LakeShore 450 Gmeter Software Version 3.8.0). To obtain high-resolution SEM images, all samples were deposited on a silicon wafer. The magnetic properties (saturation magnetization and coercivity) were measured by VSM using a known mass of sample. The composition and crystal structure of the nanoparticles was confirmed using X-ray photoelectron spectroscopy (XPS; PHI 5700 XPS with an Al Kα X-ray source), SEM (JEOL JSM 6330F Field-emission), and X-ray diffraction (XRD; Siemens D5000 X-ray diffractometer). The chemical composition of the surface layer of the iron oxide MNPs was analyzed by XPS. The characterization data are provided in the Supporting Information.

2.5. Magnetized Fibrin Gel. Magnetized fibrin scaffolds were formed and seeded the same way as their unmagnetized counterparts. Two types of MNPs were used — Fe_2O_3 (as obtained from Sigma-Aldrich) and Fe_3O_4 that were synthesized in-house (described above). In each case, Fe_2O_3 particles (with diameters <5 μm) or Fe_3O_4 MNPs (300 nm) were added to the fibrinogen-in-saline and thrombin-in-CM mixture immediately after combination of the CM and saline in a PDMS-coated Petri dish. Fe_2O_3 was added at 1, 3, 5, 7, 9, 11, and 13 wt % corresponding to 15, 45, 75, 105, 135, 165, and 195 mg, respectively. Magnetically loaded gels were assessed for stretch response to a given magnetic field for every particle load. Magnetized

scaffold were placed in a Petri dish in PBS and exposed to a 120-lb strength neodymium magnet at discrete distance intervals. Percent stretch was calculated as a measure of leading edge delta position change over total length of the construct. Force response was measured via fixation of the anterior edge of a magnetically loaded scaffold to a high-sensitivity isometric force transducer (MLT0202, ADInstruments, Colorado Springs, CO, USA) connected to a quad bridge amplifier (FE224, ADInstruments). A magnet was uniformly traversed over a fixed interval to ascertain the correlation between magnetic distance and force response. Assessment of AHM loaded with Fe_3O_4 magnetic nanoparticles was performed at 1 wt % content. Prior to addition, the MNPs were sonicated for 5 min in CM and then 1.5 mg of Fe_3O_4 was mixed with fibrinogen-in-saline and thrombin-in-CM. Cells were added to the magnetized fibrin gel in the same manner as with unmagnetized matrices.

2.6. Contractile Twitch Force. Twitch force was measured under electrical pacing at (3 V, 0.1 s) in a thermostatic (37 °C) water bath according to a previously published protocol.[14] Data capture and analysis was performed using LabChart (ADInstruments) software. The peak analysis package was used to determine baseline and twitch force values.

2.7. Immunofluorescence. Magnetized and unmagnetized AHM patches were fixed in ice-cold acetone for 10 min and trimmed to 1 cm² patches. Blocking and permeabilization was performed in 10% goat serum with 0.5% Triton X-100 at room temperature. Samples were then incubated in rabbit anticollagen type I (1:100; Abcam, ab34710), rabbit antivon Willebrand factor (vWF; 1:750; Abcam, ab6994), mouse anti-α-actinin antibody (1:200; Sigma, A7811), rabbit anti-ki67 (1:100; Abcam, ab66155), rabbit anticollagen type I (1:100; Abcam, ab34710), or rabbit anticonnexin 43 (Cx43; 1:100) antibodies for at least 2 h at room temperature. Samples were then incubated with goat antimouse and goat antirabbit secondary antibodies (1:400; AlexaFluor 488, 546 and 633, Life Technologies) and counterstained with DAPI. Images were obtained using a Nikon C2$^+$ confocal microscope (Nikon Instruments, Melville, NY, USA).

2.8. Statistics. All data are presented as mean ± standard deviation (SD). Group comparisons were made with a one-way analysis of variance (ANOVA) followed by the Bonferroni post hoc comparison test. Differences were said to be statistically significant for $p < 0.05$.

2.9. Bioreactor Design. A custom bioreactor was fabricated in house. Magnetized AHM was placed on a stage and held in place using metal clamps. A neodymium magnet was physically displaced relative
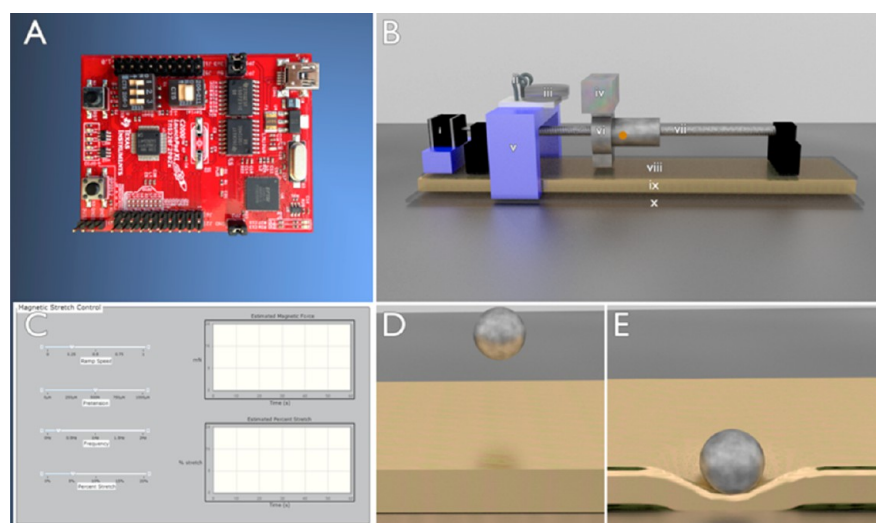
Figure 2. Prototype of the magnetic stretch bioreactor: (A) Microcontroller controls the movement of the stepper motor, (B) Schematic of bioreactor system including (i) stepper motor, which controls the motion of the magnet; (ii) Petri dish mounting hooks, which secure the Petri dish in a fixed position; (iii) Petri dish; (iv) 120 lb strength neodymium magnet; (v) Petri dish mount attached to lower base plate; (vi) threaded ballscrew, which moves when the stepper motor rotates; (vii) threaded rod attached to stepper motor; (viii) upper base plate attached to motor; (ix) memory foam absorbs the energy of vibrations from the mechanical movement of the slide and isolates the Petri dish and base layer from said vibrations; (x) lower base plate, (C) user interface for the software to run the bioreactor, (D) uncompressed memory foam, (E) compressed memory foam.

to the mAHM using a stepper-motor-driven ball screw. The rate, distance, and ramp speed of the oscillation was controlled through a custom user interface using a C2000 microcontroller (Texas Instruments, Santa Clarita, CA) to drive the stepper motor. Code Composer Studios (Texas Instruments, Santa Clarita, CA) was used to develop the user interface (UI), encode the microcontroller, and display real-time feedback. A detailed description of the bioreactor design process is included in the Supporting Information.

2.10. SEM Sample Preparation for MNPs in Fibrin Gel. The MNP-scaffold samples were imaged using SEM (LEO-1525 operating at 15 kV). Prior to imaging, we prepared our samples based on the procedure of fixation, dehydration, and drying.[34] The fibrin scaffolds with MNPs were fixed with 2.5% (v/w) glutaraldehyde for 20 h in 0.1 M PBS buffer at 4 °C. The fibrin samples were dehydrated in a gradient ethanol series (50%, 70%, 85%, 95%, and 100%) for 10 min each. The dehydrated samples were immersed and frozen in 100% t-butanol, followed by freeze-drying using a Scanvac CoolSafe 110−4 (LaboGene). The freeze-dried samples were then sputter-coated (Hummer 6.2 Sputter System; Anatech USA) with a resultant thickness of about 10 nm platinum, and then examined under SEM.

2.11. Stretch Conditioning of mAHM. The bioreactor system developed through the course of this research is capable of delivery of up to 2 hz translations with a 5 cm travel distance. Resultant magnetic interactions are based on the magnetic properties and amounts of included magnetic particle, the strength of the neodymium magnet used to induce the magnetic field, and the distance between the magnet and the magnetized AHM sample. A 15% stretch 0.5 Hz protocol was selected for stretch conditioning. The magnetic AHM was placed onto a stage with metal clamps designed to stabilize the sample a set distance (80 mm) from the resting position of the neodymium magnet. The protocol was then initiated via a custom built UI program and run for 4 h periods every day for the course of the experiment.

2.12. Ridge Analysis. Image analysis was performed using Matlab R2014a (Mathworks, Natick, MA, USA) software. We performed an adapted method of fingerprint analysis on α-actinin IHC images.[35] We applied a threshold to remove artifacts and used ridge segmentation and orientation algorithms to detect the directionality of each 4 μm^2 area of an image. Ridges were binned into 25 ranges of angles from 0 to 180° and compared using a histogram. The standard deviation of angles was used as a correlate for the tightness of the distribution.

3. RESULTS

3.1. Proof-of-Concept. Initial analysis of the magnetic scaffolds was performed on fibrin gels containing uncharacterized Fe_2O_3. The process for the magnetization and deformation of the fibrin gel is illustrated in Figure 1. Upon loading with Fe_2O_3, the fibrin gels became sensitive to magnetic fields. Higher initial loads of Fe_2O_3 led to effluent particles, which escaped from the fibrin gel. We noted the loading threshold to be ∼13 wt % Fe_2O_3 in the fibrin gel. The stretch was found to correlate positively with magnetic field strength, which is inversely related to the neodymium magnet distance from the culture chamber.

3.2. Microcontroller and UI. We chose the C2000 launchpad as the controller for our system since it is ideally suited for developmental/evaluation purposes. It contains a C2000 chipset with 60 MHz, 64 kb Flash, 12 KB RAM, 9 PWM and 4 HR PWM, 1 Capture, 22 GPIOs, 12-bit 4.6 MSPS ADC with 13 ch., SCI/UART, SPI, and I2 C. An h-bridge configuration was used to amplify the GPIO signals (baseline output of 3.3 v control signals) to higher power signals capable of driving a magnetic stepper motor. The TI C2000 chipset was designed for real-time control purposes and is widely used in motor-control applications. The LaunchPad configuration allowed for accessible transfer of commands and real-time control via a USB-UART connection. C2000 LaunchPad μCs utilize analog-to-digital converters (ADCs) that quantize continuous signals into digital outputs. Although this inherently leads to small errors and is nonideally suited for the real-time analysis of complex analog waveforms, the versatility and favorable cost of the C2000 μC system made it a suitable choice here. It was found that each stepper motor step accounted for 0.012654 mm of axial translation. A UI was developed to allow for direct control of the system through a graphical interface. For this system, the control code was written in the C programming language. Please see Figure 2 for the key components of our custom-designed bioreactor system. During initial experiments, we found that placing unmagnetized AHM

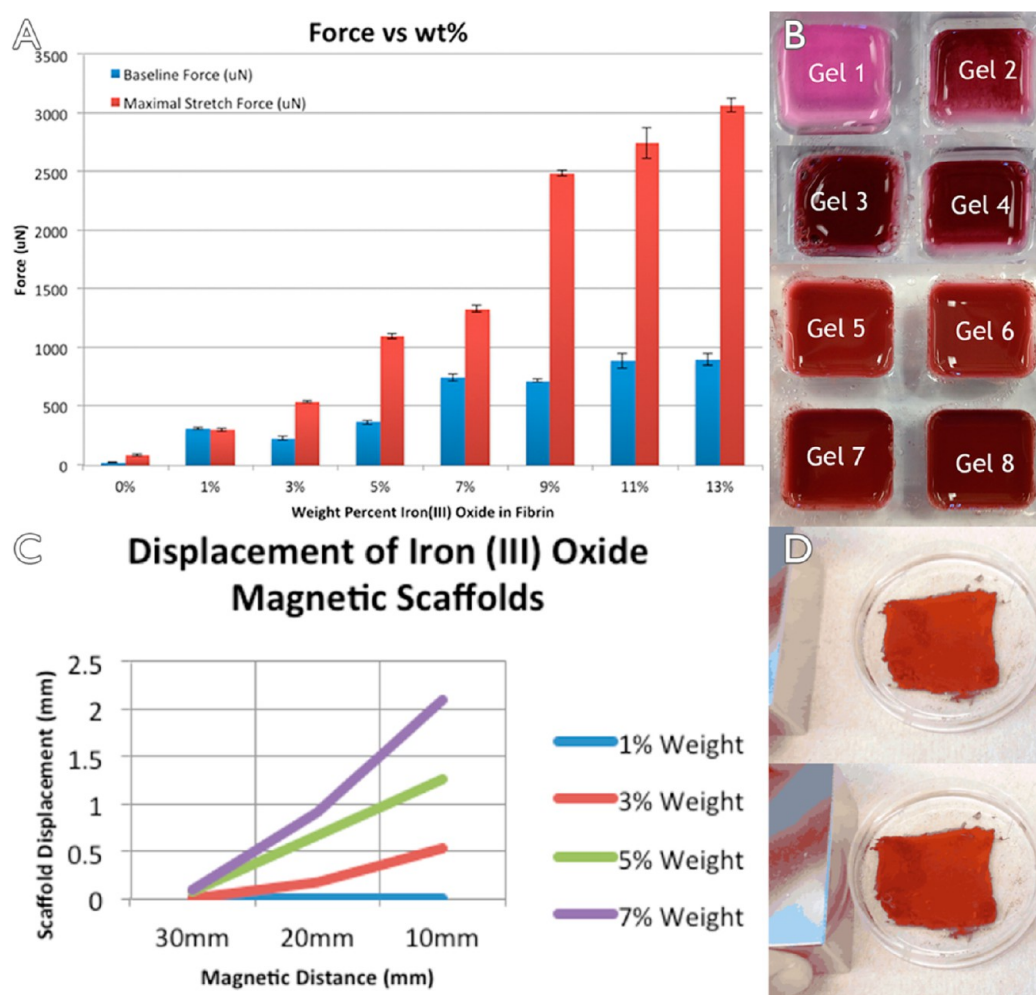**Figure 3.** (A) Magnetic forces on a patch as a function of concentration. Patches were loaded with different concentrations of Fe_2O_3, and the relative force on the rear edge of the patch was measured using a force transducer. (B) Fibrin gels with 8 different concentrations of Fe_2O_3. Gel 1−0% Fe_2O_3; Gel 2−1% Fe_2O_3; Gel 3−3% Fe_2O_3; Gel 4−5% Fe_2O_3; Gel 5−7% Fe_2O_3; Gel 6−9% Fe_2O_3; Gel 7−11% Fe_2O_3; Gel 8−13% Fe_2O_3. (C) Deformation as a function of Fe_2O_3 concentration and distance from the neodymium magnet. The graph shows the amount of deformation when a 120 lb strength neodymium magnet was placed at discrete distances from the leading edge of a patch with varying wt % of Fe_2O_3. (D) Magnetically induced deformation showing the patch stretch upon application of a magnet. Top panel: magnetic positioned away from the AHM. Lower panel: magnetic positioned close to the AHM, which gives rise to stretching of the AHM.

in the bioreactor system led to reduced functionality and cell viability. High magnitude, high frequency mechanical vibrations can cause cell detachment, cellular disruption and apoptosis in adherent cultures. It is therefore critical to insulate the culture from mechanical vibrations generated by the stepper motor and magnetic drive system. Memory foam is compressible as illustrated in Figure 2D and E. Adding a memory foam layer (Figure 2B ix) between the drive components (Figure 2B i, iv, vi, vii, and viii) and the components attached to the tissue culture (Figure 2B ii, iii, v and x) served to disperse vibration energy of the drive system and effectively eliminate unwanted vibration of the tissues cultured in the mounted Petri dish during bioreactor operation.

3.3. Magnetic Manipulation Using Fe_2O_3. Fibrin samples prepared with varying concentrations of Fe_2O_3 became darker and slightly stiffer with increasing iron content (Figure 3A). Upon application of a magnetic field, axial displacement was observed. The patches remained intact and underwent smooth deformation under magnetic load. A force curve was calibrated to determine the active forces on samples of fibrin containing different amounts of iron. A force transducer was

fixed to fibrin patches loaded with varying concentrations of Fe_2O_3 magnet. We found that an increase in Fe_2O_3 loading led to a direct increase in the forces generated at a discrete distance. Maximum deformation was assessed when the magnet was 10 mm from the leading edge. Baseline forces corresponded to the lowest magnetic forces applied during magnetic field oscillation. Higher iron content produced larger axial distortions at a constant discrete distance (Figure 3D). The patches measured 2 cm²; therefore, a 2 mm displacement of the leading edge correlated with a 10% axial stretch. Maximum stretches with 3 and 7 wt % Fe_2O_3 loading were 5 and 10% stretch, respectively.

3.4. Toxicity of Fe_2O_3. Effects of Fe_2O_3 content on AHM formation and function were assessed with regard to twitch force, appearance, and immunohistological properties (Figure 4). Measured contractile activities after 4 days of culture for control, 3 wt %, and 7 wt % Fe_2O_3 AHM were 202 ± 67 μN, 188 ± 58 μN, and 214 ± 26 μN, respectively. After 7 days of culture twitch forces for control, 3 wt %, and 7 wt % Fe_2O_3 AHM were 148 ± 47 μN, 54 ± 38 μN, and 71 ± 4 μN, respectively. At day 4 after formation, the control and the 3 and
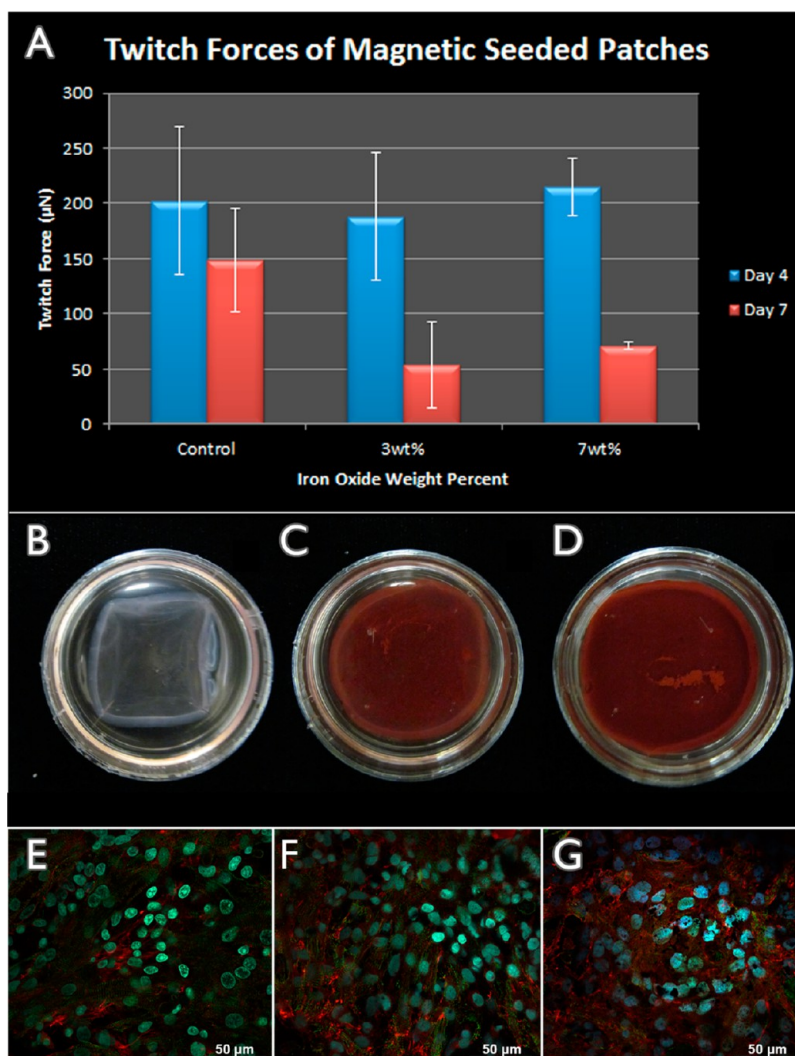
Figure 4. (A) Effects of Fe$_2$O$_3$ particles on twitch force for samples B−D. Images taken at day 8 of (E) 0, (F) 3, and (G)7 wt % Fe$_2$O$_3$ particles in heart tissue patches, respectively, showing IHC at day 8 probing for DAPI (blue), α-actinin (green), and collagen (red) for each respective concentration.

7 wt % magnetic seeded patches exhibited the same contractile activity. At day 7 after formation, there was a significant drop in functional activity of the iron-containing heart muscle. There were no apparent differences in the severity of the force drop off from day 4 to day 7 between groups containing 3 and 7 wt % iron oxide. The Fe$_2$O$_3$-containing patches exhibited a reduced definition around the edges of the patches (see Figure 4B−D) and significantly less well-defined α-actinin expression when compared with control heart muscle (see Figure 4E−G). Collagen expression appeared to be unaffected; however, no numerical assessments were applied.

3.5. Magnetic Manipulation Using Fe$_3$O$_4$ MNPs. The magnetic properties of the as-bought α-Fe$_2$O$_3$ and our synthesized Fe$_3$O$_4$ MNPs were investigated using a vibrating sample magnetometer (VSM) at 300 K. For 300 nm MNPs, the saturation magnetization (Ms) values were 82 emu/g, and coercivity values were 37 Oe, respectively (Figure S1). The bulk α-Fe$_2$O$_3$ used for the preliminary experiments to demonstrate proof-of-concept (section 3.1) had an M_s of ∼5 emu/g. Loading the scaffold (fibrin gel) with Fe$_3$O$_4$ MNPs produced a 10-fold increase in sensitivity to magnetic fields. Importantly, we were able to achieve viable stretch activity of

10−15% stretch with less than 1 wt % Fe$_3$O$_4$. Although the Fe$_3$O$_4$ MNPs were monodisperse and visually showed good loading in the fibrin gel matrix, some aggregation was observed under SEM (Figure 5).

3.6. Toxicity of Fe$_3$O$_4$ MNPs. There were reduced toxic effects associated with 1 wt % Fe$_3$O$_4$ loading up to 8 days compared to higher loadings of Fe$_2$O$_3$ required for viable stretch activity. Confocal data showed well-defined alpha actinin structures in control AHMs after 8 days of culture; the alpha actinin structures were less evident in AHMs fabricated with 1 wt % Fe$_3$O$_4$ and attributed to the presence of the MNPs (Figure 6).

For the Fe$_3$O$_4$ MNPs, there was no visible reduction in definition around the edges of the patches when comparing loaded and unloaded controls (Figure 7A). The twitch force of AHMs with 1 wt % Fe$_3$O$_4$ was 259 ± 254 μN, 298 ± 1 μN, and 189 ± 8 μN after 4, 6, and 8 days of culture, respectively; the twitch force of control AHMs for the time period were 145 ± 35 μN, 153 ± 60 μN, and 182 ± 63 μN (Figure 7D). Measured contractile activities after 4, 6, and 8 days of culture for control and 1 wt % Fe$_3$O$_4$ AHM were 259 ± 254 μN, 298 ± 1 μN, and 189 ± 8 μN, and 145 ± 35 μN, 153 ± 60 μN, and 182 ± 63
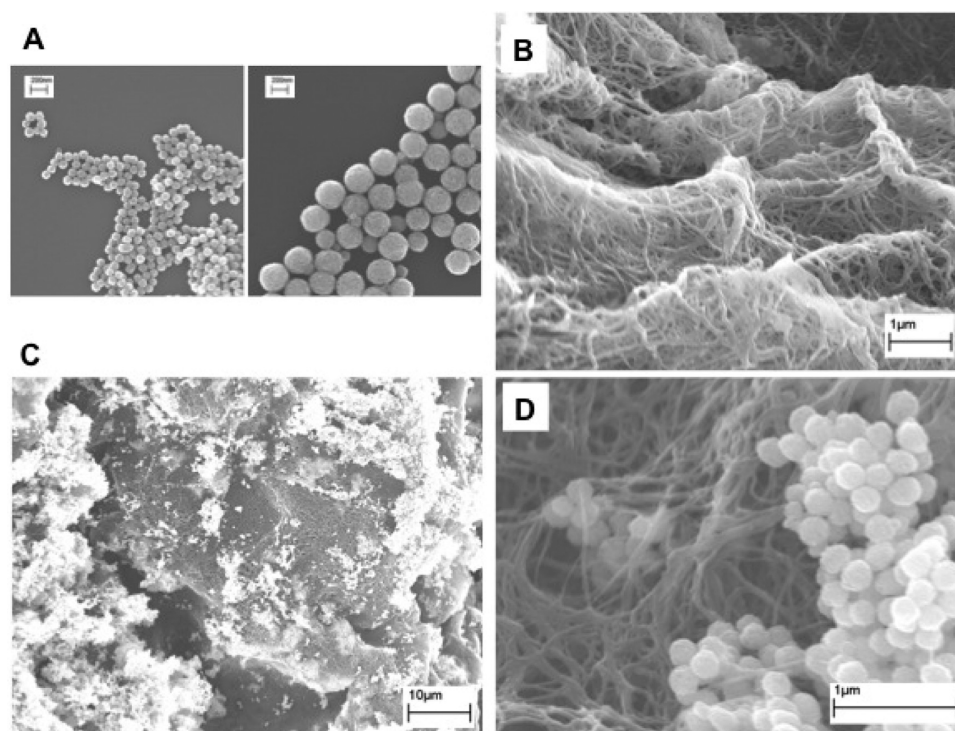
Figure 5. SEM characterization of (A) 300 nm Fe$_3$O$_4$ MNPs under different magnifications. (B) Fibrin gel without MNPs, and (C) and (D) Fibrin gel with 300 nm MNPs at different magnifications.
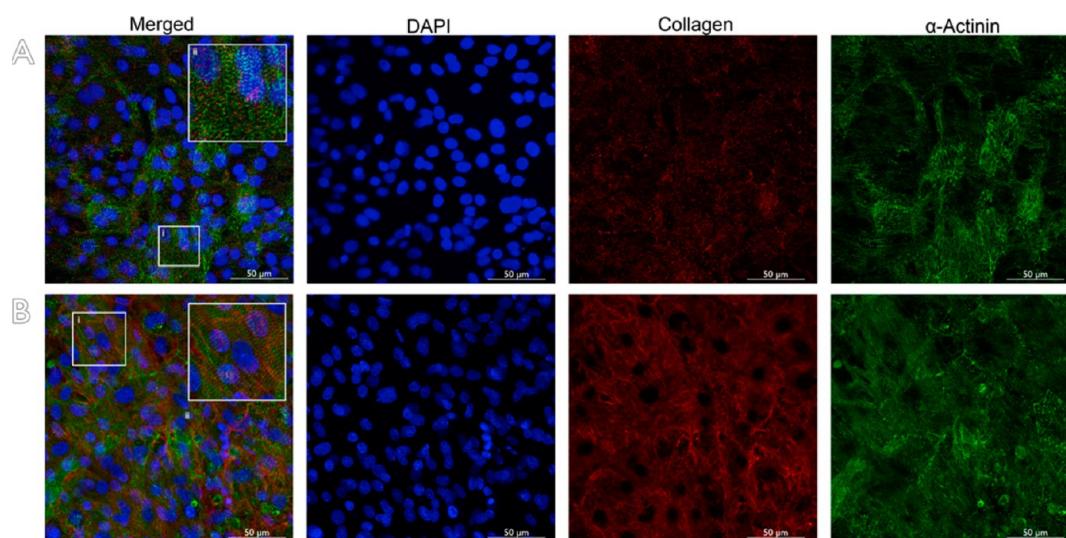

Figure 6. (A) IHC of control AHM and (B) IHC of stretch conditioned 1 wt % Fe$_3$O$_4$-loaded AHM at 8 days: DAPI (blue), α-actinin (green), and collagen (red) for each IHC image.

μN, respectively (Figure 7D). After 8 days of culture, AHM loaded with 1 wt % Fe$_3$O$_4$ typically showed similar contractile forces to untreated controls; however, contraction was generally slightly reduced at 6 days (Figure 7D).

3.7. Stretch Conditioning of Magnetic AHM. We compared the functional activity of unmagnetized AHM controls to the activity of AHM loaded with 300 nm 1 wt % Fe$_3$O$_4$ and subjected to a stretch regimen. We observed an immediate positive response to stretch stimulus after administration of a stretch protocol (Figure 7C). Patches maintained elasticity and response to magnetic stimulus after 8 days of culture (Figure 7B). Most samples exhibited a slight geometric deformation along the leading edge in the direction

of the magnetic force because of plastic deformation. This effect was slight and patches were never observed to tear or irregularly elongate. Measured contractile activities after 4, 6, and 8 days of culture for stretch-conditioned 1 wt % Fe$_3$O$_4$ AHM were 821 $\pm$ 240 μN, 424 $\pm$ 35 μN, and 127 $\pm$ 49 μN, respectively (Figure 7D). Magnetic AHM showed significantly higher twitch force activity at days 4 and 6 compared to controls.

3.8. Ridge Analysis. We analyzed the distribution of α-actinin fiber directionality using a modified ridge analysis of IHC images (Figure 8). Although several areas of the stretched mAHM appeared visibly more aligned than corresponding unstretched AHM (Figure 8E, F), a histogram analysis of ridges
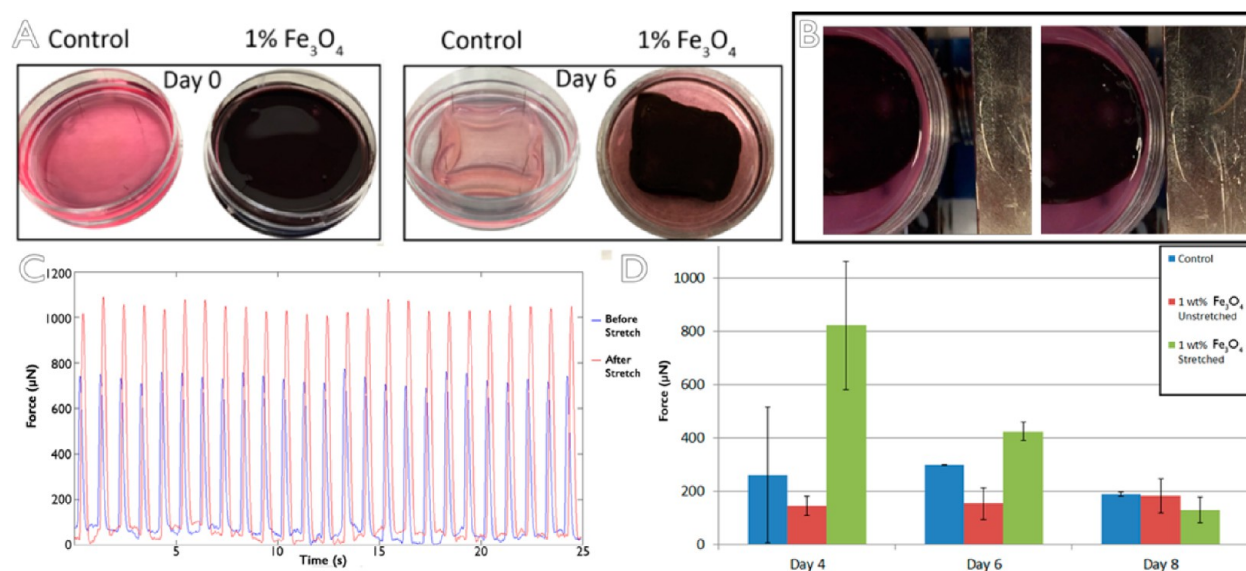
Figure 7. (A) Representative images of Fe₃O₄ free and 1 wt % AHM at days 0 and 6. (B) One hundred twenty pound magnet 50 mm from the leading edge (left) and 10 mm from the leading edge (right) of AHM loaded with 1 wt % 300 nm Fe_3O_4 particles. (C) Twitch forces at day 4 from AHM with 1 wt % 300 nm Fe_3O_4 particles immediately before and after a stretch-conditioning session. (D) Twitch forces of AHM with 1 wt % 300 nm Fe_3O_4 particles unstretched- and stretch-conditioned for 4 h daily at 0.5 Hz vs nanoparticle free AHM patches over time.
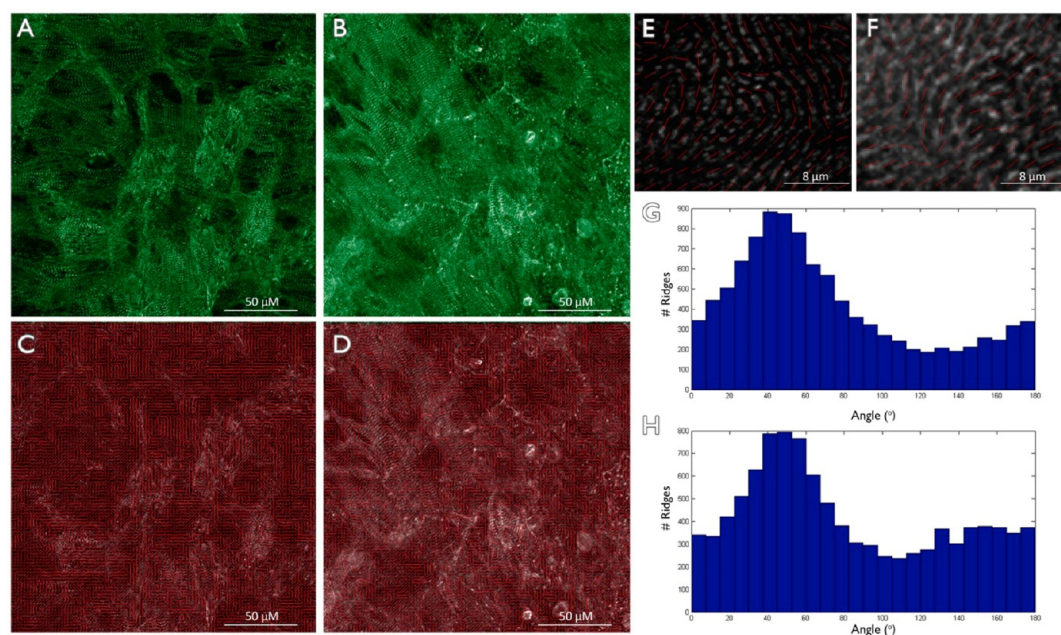

Figure 8. IHC probe for α-actinin (green) at day 8 in (A) control AHM and (B) 1 wt % Fe_3O_4-loaded AHM. (C, D) The results of an adapted ridge analysis of A and B, respectively. Each red vector represents a ridge depicting the estimated directionality of a 4 μm^2 area. (E, F) Magnified areas of C and D, respectively. (G, H) Histogram of the distribution of ridge angles in C and D, respectively.

in stretched and unconditioned AHM revealed similar distributions (Figure 8G, H). The standard deviation of the ridge angles was ±47.95° for unconditioned AHM and ±50.72° for stretched 1 wt % Fe_3O_4-loaded AHM.

4. DISCUSSION

In our preliminary studies, we used Fe_2O_3 as the ferromagnetic component of our scaffold. The as-purchased powder consisted of particles <5 μm diameter with saturation magnetization of 5 emu/g. Adding higher weight percentages of Fe_2O_3 made the scaffolds stiffer and darker in color. This preliminary assessment was based on qualitative evaluations of the mechanical integrity of the AHMs using forceps. We will quantitatively assess the mechanical properties in future studies. After a certain load, Fe_2O_3 precipitated out of the scaffold. We found that 13 wt % was the highest load at which the fibrin gel could encapsulate the powder without protocol modification. Physical stretch regimens typically involve an axial deformation of 5−15%. We were able to achieve deformations in this range using loads upward of 5 wt %. At 7 wt %, a deformation of 12% stretch was possible. Using low-magnetization-Fe_2O_3, we were able to magnetize our scaffold and induce physiologically relevant levels of stretch without saturating the scaffold (Figure 3).

Uncoated iron oxide is considered toxic in the body,[36−42] and as such, we expected a negative effect when loading with unmodified iron powder (Fe$_2$O$_3$ MNPs). After 4 days of culture, there was no difference in activity between AHM formed using Fe$_2$O$_3$-loaded scaffolds and controls (Figure 4). After 7 days of culture, however, there was a significant drop in contractile activity between AHM formed using both 3 and 7 wt % Fe$_2$O$_3$ fibrin scaffolds and controls, indicating a delayed toxic effect. We also confirmed a change in cellular expression with IHC microscopy. Controls exhibited higher levels of α-actinin and better overall organization than 3 and 7 wt % AHM constructs. Based on these studies, we concluded that the unmodified iron powder was toxic to AHMs during culture times beyond 4 days; therefore, we sought to replace unmodified iron powder with custom-fabricated MNPs, and we focused our efforts on monodispersed, high-Ms, PVP-coated Fe$_3$O$_4$ MNPs ($\sim$300 nm) to provide further support for our proof-of-concept.

Following the success of the as-purchased low-saturation magnetization (Ms) Fe$_2$O$_3$-embedded scaffold to induce stretch with toxicity during a 7 day culture period, we focused our efforts on monodispersed high-Ms Fe$_3$O$_4$ MNPs ($\sim$300 nm) to provide further support for our proof-of-concept. The Fe$_3$O$_4$ MNPs (Figure 5) exhibited a 10-fold increase in magnetization over the as-purchased Fe$_2$O$_3$ particles. Given the reduced amount of particles necessary to induce stretch, we observed reduced toxicity and improved loading efficiency using the well-characterized Fe$_3$O$_4$ nanoparticles. The Fe$_3$O$_4$-embedded scaffolds achieved 15% axial stretch using only 1 wt % of the high-Ms Fe$_3$O$_4$ MNPs.

Uncoated iron oxide, such as the as-bought Fe$_2$O$_3$, is toxic;[36−43] however, our synthesis of the Fe$_3$O$_4$ MNPs leads to the formation of a polyvinylpyrrolidone (PVP) coating on the surface, which renders them nontoxic.[44−47] The concentration of the MNPs in the scaffold is 10 mg MNPs/g scaffold. A previous study has shown that the maximum uptake in rat cardiomyocytes was 19.8 pg magnetite/cell.[48] While exposure to MNPs could potentially lead to the generation of reactive oxygen species (ROS), impaired mitochondrial function, inflammation, or DNA damage, toxicity has only been observed at 100 μg/mL uncoated MNPs.[36−49] At the levels of exposure, uptake, and threshold concentration that causes toxicity, our PVP-coated, 300 nm Fe$_3$O$_4$ MNPs should pose no concerns.

During the course of our study, we tested both Fe$_2$O$_3$ and Fe$_3$O$_4$ MNPs. The main difference between the commercial, polydispersed Fe$_2$O$_3$ and as-synthesized, monodisperse Fe$_3$O$_4$ was saturation magnetization. Consistent with previous observations,[50,51] we found that the Fe$_3$O$_4$ MNPs are 10 times more magnetic than the Fe$_2$O$_3$ MNPs (Supporting Information, pages 1−2) and therefore required a much lower concentration (1% Fe$_3$O$_4$ vs 13% Fe$_2$O$_3$) to achieve the goal of stretch activity. At 7 wt % Fe$_2$O$_3$, a deformation of 12% stretch was noted. In contrast, the Fe$_3$O$_4$-embedded scaffolds achieved a higher 15% axial stretch using a lower concentration of only 1 wt % of the high-Ms Fe$_3$O$_4$ MNPs.

Additionally, we noted that the average twitch force of AHMs fabricated using 3% Fe$_2$O$_3$ was 188 μN (Figure 4), and those fabricated using a low concentration of 1% Fe$_3$O$_4$ was 259 μN (Figure 6), after 4 days in culture. These results illustrated a decline in AHM function resulting from using Fe$_2$O$_3$ in place of Fe$_3$O$_4$. In summary, in addition to superior magnetic properties, Fe$_3$O$_4$ MNPs offer better axial stretch and contractile activity using less than a tenth of the concentration

of the Fe$_2$O$_3$ MNPs. We maintain that the difference in the saturation magnetization between Fe$_2$O$_3$ and Fe$_3$O$_4$ was largely responsible for the difference in functionality of the tissue.

Upon administration of a stretch regimen to magnetically active patches, we observed an immediate positive response in twitch force (Figure 7C). This phenomenon is typical and has been observed in other bioreactor stretch systems, although it has not, to our knowledge, been demonstrated via manipulation of a magnetically loaded scaffold. Magnetically loaded AHM maintained elasticity after being subjected to 4 h stretch regimens for 4 days. For these tests, there was no significant deformation of the patches, and the general integrity of the constructs was well-preserved after 4 days of stretch.

Importantly, we observed a functional improvement in twitch force of magnetically conditioned patches loaded with 1 wt % 300 nm Fe$_3$O$_4$ particles over unmagnetized controls at days 4 and 6 of culture. After 8 days, there appeared to be no benefit from magnetically stretching the patches. In our experience, there is a significant functional and morphological degradation of unmagnetized AHM after 8 days of culture. While the reduced benefit of stretch might be related to this general atrophy, it might also correlate to the slight toxic effect of Fe$_3$O$_4$. Judicious modification of the surfaces of the magnetic nanoparticles can be made to overcome such effects; however, any nonmagnetic coating would reduce magnetic efficiency (but only minimally under optimal conditions). Further optimization to balance particle load, MNP composition, and magnet strength might improve the beneficial time period of stretch conditioning using these noncontact magnetic systems.

The focus of this manuscript is to demonstrate the use of MNP-embedded scaffolds to impart functionality to AHM using a noncontact stretch reactor, and we have demonstrated its success. The toxicity of MNPs has been evaluated in the following cell culture studies, based on which we believe that MNPs in our studies will not evoke a significant toxic effect during in vitro and in vivo culture:

(a) In a study by Xiong et al.,[51] the viability of neonatal rat cardiomyocytes incubated with 0.01, 0.1, and 0.5 mg/mL Fe$_2$O$_3$@DMSA (2, 3-dimercaptosuccinic acid) MNPs was 94.0 $\pm$ 9.2%, 94.6 $\pm$ 9.2%, and 96.2 $\pm$ 7.1%, indicating no/low toxicity.

(b) In work conducted by Gaihre et al.,[52] the uptake of uncoated MNPs was higher as compared to gelatin-coated Fe$_3$O$_4$ MNPs, leading to lower cell viability that was dose-dependent.

(c) Lewis and co-workers used cell-seeded scaffolds, such as collagen gels, to model a 3D tissue environment.[53] In their study, the cell viability was not affected over the 24 h period tested for size (100, 200, 500 nm), composition (Fe$_2$O$_3$ vs Fe$_3$O$_4$), or presence of magnetic field (the MNPs were under a magnetic field for high uptake). The 500 nm Fe$_2$O$_3$ MNPs had the lowest uptake and penetration.

An analysis of α-actinin fibers (Figure 8) revealed little difference in overall alignment before and after stretch conditioning. Researchers have reported enhanced α-actinin fiber alignment and cellular elongation along the direction of stretch; however, a preliminary examination revealed a remarkably similar distribution of fiber angles in our case (Figure 8G, H). Although some discrete analysis of local fibers showed better alignment after stretch on a small scale (Figure 8E, F), there was no large change in polarity toward the

direction of stretch. The lack of an increased alignment may be explained by a pre-existing polarity. The ridge angle histogram for the unconditioned AHM reveals a distribution with a clear peak centered at 50° (Figure 8G). Fibrin gel is flexible. During spontaneous contraction, unmodified AHM contracts visibly toward the center of the patch resulting in displacement of fibrin gel. The forces generated during contraction may be significant enough to spontaneously align fibers and explain a pre-existing polarity. There may be an undetected enhancement of polarity following stretch. The center region of AHM is least affected by spontaneous contraction and may yield interesting information regarding pre-existing polarity. Further, an analysis of multiple regions of each sample is necessary to determine whether observed polarity is regional or uniform within each sample of AHM.

Earlier work in the field of cardiac tissue engineering has demonstrated a positive correlation between stretch and 3D heart muscle function.[15,16] A seminal publication in the field demonstrated the concept of noncontact stretch bioreactors for 3D heart muscle.[18] The current study builds on this prior work and describes a new noncontact stretch bioreactor to condition 3D heart muscle. Adding to our existing body of knowledge, this study demonstrates an increase in twitch force of contraction in response to noncontact stretch, thereby representing advancement in the field of heart muscle tissue engineering.

5. SUMMARY

We developed a novel noncontact stretch-based bioreactor to induce mechanical stimulation of tissue-engineered cardiac muscle using a scaffold system embedded with MNPs. This system is capable of delivering axial stretch via application of an oscillating magnetic field to a magnetized AHM construct. Our initial success with bulk as-purchased iron oxide as the magnetic component led to the use of highly magnetic custom-synthesized Fe_3O_4 MNPs in the scaffold matrix. In both cases, the system delivered physiologically relevant stretch without causing undue stress on the constructs. We were able to improve the twitch force of the AHM constructs through conditioning in a noncontact magnetic stretch bioreactor system.

ASSOCIATED CONTENT

Ⓢ Supporting Information

The Supporting Information is available free of charge on the ACS Publications website at DOI: 10.1021/acsbiomaterials.6b00375.

Additional info regarding magnetic properties of the reported nanoparticles and design considerations for the stretch bioreactor system (PDF)

AUTHOR INFORMATION

Corresponding Author
*E-mail: rkbirla@uh.edu.

Author Contributions

The manuscript was written through contributions of all authors. All authors have given approval to the final version of the manuscript.

Notes

The authors declare no competing financial interest.

ABBREVIATIONS

MNP, magnetic nanoparticle
AHM, 3D artificial heart muscle
mAHM, magnetic 3D artificial heat muscle
MSB, magnetic stretch bioreactor
DS, dissociation solution
CM, culture media

REFERENCES

(1) Mendis, S.; Puska, P.; Norrving, B. *Global Atlas on Cardiovascular Disease Prevention and Control: Policies, Strategies, and Interventions*; World Health Organization, World Heart Federation, and World Stroke Organization: Geneva, Switzerland, 2011; *vi*155

(2) Mozaffarian, D.; Benjamin, E. J.; Go, A. S.; Arnett, M. J.; Blaha, M. J.; Cushman, M.; de Ferranti, S.; Despres, J.-P.; Fullerto, H. J.; Howard, V. J.; et al. Heart Disease and Stroke Statistics−2015 Update: A Report From the American Heart Association. *Circulation* **2015**, *131* (4), E29−E322.

(3) Eschenhagen, T.; Fink, C.; Remmers, U.; Scholz, H.; Wattchow, J.; Weil, J.; Zimmermann, W.; Dohmen, H. H.; Schafer, H.; Bishopric, N.; Wakatsuki, T.; Elson, E. L. Three-dimensional reconstitution of embryonic cardiomyocytes in a collagen matrix: a new heart muscle model system. *FASEB J.* **1997**, *11* (8), 683−694.

(4) Freed, L. E.; Vunjak-Novakovic, G. Microgravity tissue engineering. *In Vitro Cell. Dev. Biol.: Anim.* **1997**, *33* (5), 381−5.

(5) Birla, R. *Introduction to Tissue Engineering: Applications and Challenges*, 1st ed.; Wiley−IEEE Press: New York, 2014.

(6) Hogan, M.; Mohamed, M.; Tao, Z. W.; Gutierrez, L.; Birla, R. Establishing the framework to support bioartificial heart fabrication using fibrin-based three-dimensional artificial heart muscle. *Artif. Organs* **2015**, *39* (2), 165−71.

(7) Huang, Y. C.; Khait, L.; Birla, R. K. Contractile three-dimensional bioengineered heart muscle for myocardial regeneration. *J. Biomed. Mater. Res., Part A* **2007**, *80* (3), 719−731.

(8) Khait, L.; Birla, R. K. Effect of thyroid hormone on the contractility of self-organized heart muscle. *In Vitro Cell. Dev. Biol.: Anim.* **2008**, *44* (7), 204−13.

(9) Akins, R. E.; Boyce, R. A.; Madonna, M. L.; Schroedl, N. A.; Gonda, S. R.; McLaughlin, T. A.; Hartzell, C. R. Cardiac organogenesis in vitro: reestablishment of three-dimensional tissue architecture by dissociated neonatal rat ventricular cells. *Tissue Eng.* **1999**, *5* (2), 103−18.

(10) Bursac, N.; Papadaki, M.; Cohen, R. J.; Schoen, F. J.; Eisenberg, S. R.; Carrier, R.; Vunjak-Novakovic, G.; Freed, L. E. Cardiac muscle tissue engineering: toward an in vitro model for electrophysiological studies. *Am. J. Physiol.* **1999**, *277* (2:Pt2), H433−444.

(11) Carrier, R. L.; Papadaki, M.; Rupnick, M.; Schoen, F. J.; Bursac, N.; Langer, R.; Freed, L. E.; Vunjak-Novakovic, G. Cardiac tissue engineering: cell seeding, cultivation parameters, and tissue construct characterization. *Biotechnol. Bioeng.* **1999**, *64* (5), 580−9.

(12) Li, R. K.; Yau, T. M.; Weisel, R. D.; Mickle, D. A.; Sakai, T.; Choi, A.; Jia, Z. Q. Construction of a bioengineered cardiac graft. *J. Thorac. Cardiovasc. Surg.* **2000**, *119* (2), 368−75.

(13) Zimmermann, W. H.; Fink, C.; Kralisch, D.; Remmers, U.; Weil, J.; Eschenhagen, T. Three-dimensional engineered heart tissue from

neonatal rat cardiac myocytes. *Biotechnol. Bioeng.* **2000**, *68* (1), 106−114.

(14) Tao, Z. W.; Mohamed, M.; Hogan, M.; Gutierrez, L.; Birla, R. K. Optimizing a spontaneously contracting heart tissue patch with rat neonatal cardiac cells on fibrin gel. *J. Tissue Eng. Regener. Med.* **2014**, DOI: 10.1002/term.1895.

(15) Fink, C.; Ergun, S.; Kralisch, D.; Remmers, U.; Weil, J.; Eschenhagen, T. Chronic stretch of engineered heart tissue induces hypertrophy and functional improvement. *FASEB J.* **2000**, *14* (5), 669−679.

(16) Akhyari, P.; Fedak, P. W.; Weisel, R. D.; Lee, T. Y.; Verma, S.; Mickle, D. A.; Li, R. K. Mechanical stretch regimen enhances the formation of bioengineered autologous cardiac muscle grafts. *Circulation* **2002**, *106* (12 Suppl 1), I137−142.

(17) Riehl, B. D.; Park, J. H.; Kwon, I. K.; Lim, J. Y. Mechanical stretching for tissue engineering: two-dimensional and three-dimensional constructs. *Tissue Eng., Part B* **2012**, *18* (4), 288−300.

(18) Boublik, J.; Park, H.; Radisic, M.; Tognana, E.; Chen, F.; Pei, M.; Vunjak-Novakovic, G.; Freed, L. E. Mechanical properties and remodeling of hybrid cardiac constructs made from heart cells, fibrin, and biodegradable, elastomeric knitted fabric. *Tissue Eng.* **2005**, *11* (7−8), 1122−32.

(19) Cooper, Gt. Cardiocyte adaptation to chronically altered load. *Annu. Rev. Physiol.* **1987**, *49*, 501−18.

(20) Salameh, A.; Karl, S.; Djilali, H.; Dhein, S.; Janousek, J.; Daehnert, I. Opposing and synergistic effects of cyclic mechanical stretch and alpha- or beta-adrenergic stimulation on the cardiac gap junction protein Cx43. *Pharmacol. Res.* **2010**, *62* (6), 506−13.

(21) Gwak, S. J.; Bhang, S. H.; Kim, I. K.; Kim, S. S.; Cho, S. W.; Jeon, O.; Yoo, K. J.; Putnam, A. J.; Kim, B. S. The effect of cyclic strain on embryonic stem cell-derived cardiomyocytes. *Biomaterials* **2008**, *29* (7), 844−56.

(22) Mahmoudi, M.; Simchi, A.; Milani, A. S.; Stroeve, P. Cell toxicity of superparamagnetic iron oxide nanoparticles. *J. Colloid Interface Sci.* **2009**, *336* (2), 510−8.

(23) Singh, N.; Jenkins, G. J.; Asadi, R.; Doak, S. H. Potential toxicity of superparamagnetic iron oxide nanoparticles (SPION). *Nano Rev.* **2010**, *1*, 1.

(24) Haisler, W. L.; Timm, D. M.; Gage, J. A.; Tseng, H.; Killian, T. C.; Souza, G. R. Three-dimensional cell culturing by magnetic levitation. *Nat. Protoc.* **2013**, *8* (10), 1940−9.

(25) Sasaki, T.; Iwasaki, N.; Kohno, K.; Kishimoto, M.; Majima, T.; Nishimura, S.; Minami, A. Magnetic nanoparticles for improving cell invasion in tissue engineering. *J. Biomed. Mater. Res., Part A* **2008**, *86* (4), 969−978.

(26) Thevenot, P.; Sohaebuddin, S.; Poudyal, N.; Liu, J. P.; Tang, L. Magnetic Nanoparticles to Enhance Cell Seeding and Distribution in Tissue Engineering Scaffolds. *Proc. IEEE Conf Nanotechnol.* **2008**, *2008*, 646−9.

(27) Tseng, H.; Gage, J. A.; Raphael, R. M.; Moore, R. H.; Killian, T. C.; Grande-Allen, K. J.; Souza, G. R. Assembly of a three-dimensional multitype bronchiole coculture model using magnetic levitation. *Tissue Eng., Part C* **2013**, *19* (9), 665−675.

(28) Frimpong, R. A.; Hilt, J. Z. Magnetic nanoparticles in biomedicine: synthesis, functionalization and applications. *Nanomedicine (London, U. K.)* **2010**, *5* (9), 1401−14.

(29) Huang, S. H.; Juang, R. S. Biochemical and biomedical applications of multifunctional magnetic nanoparticles: a review. *J. Nanopart. Res.* **2011**, *13* (10), 4411−30.

(30) Sapir, Y.; Polyak, B.; Cohen, S. Cardiac tissue engineering in magnetically actuated scaffolds. *Nanotechnology* **2014**, *25* (1), 014009.

(31) Dobson, J.; Cartmell, S. H.; Keramane, A.; El Haj, A. J. Principles and design of a novel magnetic force mechanical conditioning bioreactor for tissue engineering, stem cell conditioning, and dynamic in vitro screening. *IEEE Trans Nanobioscience.* **2006**, *5* (3), 173−7.

(32) Birla, R. K.; Huang, Y. C.; Dennis, R. G. Development of a novel bioreactor for the mechanical loading of tissue-engineered heart muscle. *Tissue Eng.* **2007**, *13* (9), 2239−48.

(33) Xuan, S. H.; Wang, Y. X. J.; Yu, J. C.; Cham-Fai Leung, K. Tuning the Grain Size and Particle Size of Superparamagnetic Fe3O4Microparticles. *Chem. Mater.* **2009**, *21* (21), 5079−5087.

(34) Khantamat, O.; Li, C. H.; Yu, F.; Jamison, A. C.; Shih, W. C.; Cai, C. Z.; Lee, T. R. Gold Nanoshell-Decorated Silicone Surfaces for the Near-Infrared (NIR) Photothermal Destruction of the Pathogenic Bacterium E. faecalis. *ACS Appl. Mater. Interfaces* **2015**, *7* (7), 3981−93.

(35) Hong, L.; Wan, Y.; Jain, A. Fingerprint image enhancement: algorithm and performance evaluation. *IEEE Trans. Pattern Anal. Mach. Intell.* **1998**, *20* (8), 13.

(36) Mahmoudi, M.; Azadmanesh, K.; Shokrgozar, M. A.; Journeay, W. S.; Laurent, S. Effect of Nanoparticles on the Cell Life Cycle. *Chem. Rev.* **2011**, *111*, 3407−32.

(37) Haga, N.; Haneda, K. Paramecium as a bioassay system for elucidation of cytotoxiccity and biocompatibility of nanoparticles: effects of carbon nanofibers on proliferation and survival. *Jpn. J. Protozool.* **2007**, *40* (2), 139−146.

(38) Shoup, C. S.; Boykin, J. T. The insensitivity of Paramecium to cyanide and effects of iron on respiration. *J. Gen. Physiol.* **1931**, *15*, 107−118.

(39) Shen, Y.; Huang, Z.; Liu, X.; Qian, J.; Xu, J.; Yang, X.; Sun, A.; Ge, J. Iron-induced myocardial injury: an alarming side effect of superparamagnetic iron oxide. *nanoparticles* **2015**, *19*, 2032−205.

(40) Mahmoudi, M.; Simchi, A.; Milani, A. S.; Stroeve, P. Cell toxicity of superparamagnetic iron oxide nanoparticles. *J. Colloid Interface Sci.* **2009**, *336* (2), 510−8.

(41) Singh, N., Jenkins, G. J. S., Asadi, R., Doak, S. H. Potential toxicity of superparamagnetic iron oxide nanoparticles (SPION). *Nano Rev.* **2010**, *1*, DOI: 10.3402/nano.v1i0.5358.

(42) Shubayev, V. I.; Pisanic, T. R.; Jin, S. Magnetic nanoparticles for theragnostics. *Adv. Drug Delivery Rev.* **2009**, *61* (6), 467−77.

(43) Shen, Y.; Huang, Z.; Liu, X.; Qian, J.; Xu, J.; Yang, X.; Sun, A.; Ge, J. Iron-induced myocardial injury: an alarming side effect of superparamagnetic iron oxide nanoparticles. *J. Cell Mol. Med.* **2015**, *19* (8), 2032−5.

(44) Wang, G.; Chang, Y.; Wang, L.; Wei, Z.; Kang, J.; Sang, L.; Dong, X.; Chen, G.; Wang, H.; Qi, M. Preparation and characterization of PVPI-coated Fe3O4 nanoparticles as an MRI contrast agent. *J. Magn. Magn. Mater.* **2013**, *340*, 57−60.

(45) Lu, A. H.; Salabas, E. L.; Schuth, F. Magnetic nanoparticles: synthesis, protection, functionalization, and application. *Angew. Chem., Int. Ed.* **2007**, *46*, 1222−44.

(46) Frey, N. A.; Peng, S.; Cheng, K.; Sun, S. Magnetic nanoparticles: synthesis, functionalization, and applications in bioimaging and magnetic energy storage. *Chem. Soc. Rev.* **2009**, *38*, 2532−42.

(47) Deng, H.; Li, X.; Peng, Q.; Wang, X.; Chen, J.; Li, Y. Monodisperse magnetic single-crystal ferrite microspheres. *Angew. Chem., Int. Ed.* **2005**, *44*, 2782−5.

(48) Ito, A. Tissue engineering using magnetic nanoparticles. *Igaku no Ayumi.* **2009**, *230* (8), 517−521.

(49) Shubayev, V. I.; Pisanic, T. R.; Jin, S. Magnetic nanoparticles for theragnostics. *Adv. Drug Delivery Rev.* **2009**, *61* (6), 467−77.

(50) Islam, M. S.; Kurawaki, J.; Kusumoto, Y.; Abdulla-Al-Mamun, M.; Bin Mukhlish, M. Z. Hydrothermal novel synthesis of neck-structured hyperthermia-suitable magnetic (Fe3O4, γ-Fe2O3 and α-Fe2O3) nanoparticles. *J. Sci. Res. (Rajshahi, Bangladesh)* **2012**, *4* (1), 99−107.

(51) Xiong, F.; Wang, H.; Feng, Y.; Li, Y.; Hua, X.; Pang, X.; Zhang, S.; Song, L.; Zhang, Y.; Gu, N. Cardioprotective activity of iron oxide nanoparticles. *Sci. Rep.* **2015**, *5*, 8579.

(52) Gaihre, B.; Lee, Y. H.; Khil, M. S.; Yi, H. K.; Kim, H. Y. In-vitro cytotoxicity and cell uptake study of gelatin-coated magnetic iron oxide nanoparticles. *J. Microencapsulation* **2011**, *28* (4), 240−247.

(53) Lewis, E. E. L.; Child, H. W.; Hursthouse, A.; Stirling, D.; McCully, M.; Paterson, D.; Mullin, M.; Berry, C. C. The influence of particle size and static magnetic fields on the uptake of magnetic nanoparticles into three dimensional cell-seeded collagen gel cultures. *J. Biomed. Mater. Res., Part B* **2015**, *103* (6), 1294−301.